

Field Ionization and Field Emission with Intense, Single-cycle THz Pulses

Need to replace with my own title

by

© Yunxiao Wang

A thesis submitted to the
School of Graduate Studies
in partial fulfilment of the
requirements for the degree of
Anqing, Anhui, China

B.S. in Physics University of Science and Technology of China May 2009

Memorial University of Newfoundland

Doctor of Philosophy

St. John's

Newfoundland

Department of Physics August, 2016

Acknowledgements

Put your acknowledgements here...

“Intellectual and practical assistance, advice, encouragement and sources of monetary support should be acknowledged. It is appropriate to acknowledge the prior publication of any material included in the thesis either in this section or in the introductory chapter of the thesis.”

— MUN School of Graduate Studies

Contents

Acknowledgements	ii
List of Tables	vii
List of Figures	x
1 Development of Cells with Metal End Windows	1
1.1 Overview	1
1.2 Wall Relaxation of ^3He	3
1.2.1 Relaxation on Glass Surfaces	3
1.2.2 Relaxation on Metal Surfaces	7
1.3 Test Cell Fabrication	9
1.3.1 Overview	9
1.3.2 Glass-Metal Seal	11
1.3.3 Mechanical Polishing and Electropolishing	12
1.3.4 Electroplating	14
1.3.5 Final Assembly of the Cell	14
1.4 Cell Fill Procedure	16

1.4.1	Cell Fill Preparation	16
1.4.2	Cell Fill	18
1.5	Experimental Setup and Procedure	20
1.5.1	Pickup Coils	20
1.5.2	Gradient Coils	21
1.5.3	Laser Setup	23
1.5.4	PNMR Losses and Corrected Lifetime	24
1.6	Relaxation Measurement Results and Discussion	30
1.6.1	Gold Coated Spherical Cell	31
1.6.2	Gold Coated Spool Pieces	33
1.6.3	Vertical Cells	34
1.6.4	Horizontal Cells	38
1.6.5	GE180 Cells	40
1.6.6	Titanium Tubes	42
	Bibliography	43
	A Appendix title	54

List of Tables

1.1 Shown are the fill information, design and maximum measured lifetime of the test cells. Fill type is the method used to clean the gas. † indicates the maximum lifetime was obtained at an elevated position. Although canary glass is not metal, it is listed in the column of metal for Tweety and Sylvester for the sake of keeping the structure of the table simple.	32
---	----

List of Figures

1.1	Shown on the left is a glass-to-metal-to-glass seal. The metal tube is 5" long by 1" outer diameter. The glass is wetted onto the knife-edge of copper on both ends. Shown on the right is a finished cell with the glass-to-metal-to-glass tube attached.	10
1.2	Glass-to-metal seals survived pressure higher than 20 atm.	11
1.3	Electropolishing [28]	13
1.4	Shown left is the inner surface of a gold coated OFHC copper tube. Shown right is a OFHC copper tube without coating.	15
1.5	Ultrasonic cleaner with 3 tubes being cleaned.	15
1.6	Shown is the design of a typical string for our test cells.	17
1.7	A diagram of a Pyrex string with a cell and a retort attached while connected to the gas system through the bellows. Adapted from Matyas [44].	18
1.8	Diagram of the coils. Adapted from Zheng [68].	22
1.9	Optics for spin-exchange optical pumping. Adapted from Zheng [68].	25
1.10	PNMR setup.	26
1.11	A PNMR signal taken with gold coated test cell.	28
1.12	3 spindowns of the cell GoldenVec1 each with a different sampling rate.	29

1.13 A linear fit to extract lifetime corrected for relaxation due to PNMR losses.	30
1.14 A diagram of target cell with metal end windows.	31
1.15 A picture of Gold Maiden, generally referred to as the “spool piece”.	33
1.16 Design and picture of Goldfinger.	35
1.17 The observed degradation of lifetime for Goldfinger (left) and Cupid (right). Shown in each of the two plots were several spindowns at different stage during the tests. The initial amplitude of the spindowns were scaled to 1 for better comparison of lifetime.	36
1.18 A picture of GoldenEye, the only test cell made with a valve.	37
1.19 Four spindowns of Goldrush before elevating the cell. All four measurements display similar lifetime with no obvious sign of degradation.	38
1.20 Shown on the right is the inhomogeneities vs. vertical distance from the center of the field. Shown on the left is the cell Goldrush with relaxation time due to field inhomogeneities as displayed on the right.	39
1.21 Design of the horizontal cell GoldenVec.	39

Chapter 1

Development of Cells with Metal End Windows

1.1 Overview

Electron scattering experiments at JLab have traditionally used ${}^3\text{He}$ targets made of glass due to the compatibility with spin-exchange optical pumping, the capability to be shaped into desired geometries through glass blowing, and the excellent nuclear spin relaxation properties.

During 12 GeV running at JLab, polarized ${}^3\text{He}$ experiments are planned that will be run at much higher luminosities than has previously been the case. The maximum current used before the upgrade was $15\mu\text{A}$, while future ${}^3\text{He}$ experiments will be run at up to $60\mu\text{A}$. We believe an all-glass target cell might survive long enough for an experiment with $30\mu\text{A}$, but it is unlikely to survive at $60\mu\text{A}$. A natural solution would be to replace the thin glass window (where electron beam enters and exits the target

cell) with a material with higher strength and good spin-relaxation properties.

Deninger *et al.* [56] from the Mainz group showed relaxation time of various metal surfaces: Mg (6 h), Al (6 h), Zn(12 h) etc. Gold caught our attention in particular, because it has a relatively long relaxation time of 20 h. This relaxation time was measured with the entire glass surface coated with gold, thus the area of gold surface was much larger than what will be needed for target windows. In addition, while the coating process made sure of the chemical purity, it did not make effort in ensuring the microscopic smoothness, which means the surface area was further increased. Therefore one would expect a even longer relaxation time with a smooth and smaller metallic surface. In light of this, our group has tested 19 cells with various geometries and materials, most of which incorporated an OFHC (oxygen-free high thermal conductivity) copper tube with gold coating. Towards the end of my work, we achieved a 15.6 h relaxation time with a Pyrex cell that had a 5" long by 1" gold coated copper tube attached horizontally. By extrapolating the relaxation rate due to gold surface from this result, we believe the relaxation rate introduced by small metal windows in a target cell will be less than $1/135 \text{ hr}^{-1}$. To the best of our knowledge, our group was the first to have proved the potential of incorporating metal to target cells in the presence of alkali vapor.

1.2 Wall Relaxation of ^3He

1.2.1 Relaxation on Glass Surfaces

Fitzsimmons and Walters have studied surface-induced spin-lattice relaxation times as a function of temperature for ^3He gas in glass containers [31]. There are mainly two categories of wall relaxation mechanisms: ^3He adsorption onto the glass surface and the permeation of ^3He into glass. The latter mechanism can be greatly reduced by using impermeable aluminosilicate glass such as GE180.

Timsit and Daniels [1] then studied surface relaxation on a great number of common materials and presented a phenomenological model to describe the relaxation processes. For permeable glasses, the relaxation is determined by absorption of gas in the surface layer of the glass and by the paramagnetic-impurity contents of the glass. The surface adsorption of ^3He near paramagnetic sites on the walls also contributes to the nuclear relaxation. Relaxation due to absorption for permeable glasses will be discussed first below.

The diffusion coefficient D of a noble gas in a glass can be calculated with the following equation:

$$D = D_0 e^{-E_{diff}/kT} \quad (1.1)$$

where E_{diff} is the activation energy for diffusion and D_0 is a constant. The diffusion coefficient can also be expressed with the mean diffusion jump distance of ^3He atom in the glass $\langle \Delta r \rangle$ as:

$$D = \frac{\langle \Delta r \rangle^2}{6\tau} \quad (1.2)$$

with τ being the mean time between diffusion jumps

$$\tau = \tau_0 e^{E_{diff}/kT} \quad (1.3)$$

where $\tau_0 = \langle \Delta r \rangle^2 / 6D_0$.

Let n_g be the number of atoms dissolved in the surface layer of mean thickness $\langle \Delta r \rangle$, the rate at which ${}^3\text{He}$ atoms enter and leave the surface layer of the glass is then $n_g/6\tau$ [1]. n_g should be proportional to the solubility S of ${}^3\text{He}$ in the glass, so for a spherical cell

$$n_g = \frac{6NkT\langle \Delta r \rangle S}{d} \quad (1.4)$$

where d is the diameter of the cell, N is the total number of free ${}^3\text{He}$ atoms.

For most trapping sites in the glass, the intrinsic relaxation time T_i is longer than τ which is the time it takes for ${}^3\text{He}$ to leave the $\langle \Delta r \rangle$ layer. However, T_i for a paramagnetic site is shorter than τ , thus will completely relax the nuclear spin of a ${}^3\text{He}$ atom. The relaxation time of ${}^3\text{He}$ in permeable glass cells is controlled by absorption of the atoms in the surface layer at paramagnetic sites. The average nuclear relaxation time of a ${}^3\text{He}$ trapped in the glass close to a Fe^{3+} ion (one common type of paramagnetic impurity in glass) is [6]:

$$\frac{1}{T_i} \approx \frac{3}{5} \frac{\mu_{He}^2 \mu_B^2 g^2}{\hbar^2 b^6} \frac{T_{Fe}}{1 + \omega_0^2 T_{Fe}^2} \quad (1.5)$$

where μ_{He} is the nuclear dipole moment of ${}^3\text{He}$, μ_B is the Bohr magneton, g is the g factor of the Fe^{3+} (${}^6S_{5/2}$) ion, b is the distance between the spins, and T_{Fe} is the relaxation time of a Fe^{3+} ion in glass. Taking b as 1 \AA and g as 5.9 [?], T_i is $\sim 10^{-11} \text{ s}$, which is 10 times smaller than the shortest τ .

Even a small amount of paramagnetic impurities among the trapping sites in the glass could potentially provide dominating contribution on the ${}^3\text{He}$ spin relaxation.

Assuming during the random walk of ${}^3\text{He}$ atom in the glass, there are on average β atoms in its vicinity, and atom fraction of paramagnetic impurities is $N_{impurity}$, the relaxation time due to absorption is if $T_i \ll \tau$:

$$T_{ab} = \frac{6N\tau}{\beta N_{impurity} n_g} \quad (1.6)$$

For impermeable glasses such as GE180, the relaxation rate due to absorption into the glass walls is typically negligible. The dominating relaxation mechanism here is adsorption of ${}^3\text{He}$ on the glass wall in vicinity of a paramagnetic site.

The sticking time τ_s is given by Frenkel's Law [32]:

$$\tau_s = \tau_{s0} e^{E_{ad}/kT} \quad (1.7)$$

where τ_{s0} is on the order of 10^{-13} s for most solid surfaces [32], E_{ad} is the adsorption energy. At room temperature, we have $\tau_s \sim \tau_{s0} \sim 10^{-13}$ s. The number of atoms hitting the wall per unit time and unit area is given by $\frac{1}{4}n\bar{v}$, where n is the number density of ${}^3\text{He}$ gas and \bar{v} is the mean velocity. For a spherical cell with diameter d , the number of atoms adsorbed on the wall is

$$n'_g = \frac{3N\bar{v}\tau_s}{2d} \quad (1.8)$$

The intrinsic relaxation time T'_i of a ${}^3\text{He}$ near a paramagnetic site on the wall is much longer than the sticking time τ_s . The average number of collisions required to depolarize ${}^3\text{He}$ is T'_i/τ_s , thus the relaxation time due to adsorption is

$$T_{ad} = \frac{NT'_i}{N_{impurity}n'_g} \quad (1.9)$$

The total relaxation rate is the sum of that due to adsorption and absorption (for permeable glasses):

$$\frac{1}{T_{wall}} = \frac{1}{T_{ad}} + \frac{1}{T_{ab}} \quad (1.10)$$

Substitute Eq. 1.3, 1.4 into Eq. 1.6 and Eq. 1.7, 1.8 into Eq. 1.9, the wall relaxation rate can be written as

$$\frac{1}{T_{wall}} = \frac{\beta N_{impurity} k T \langle \Delta r \rangle S}{d \tau_0} e^{-E_{diff}/kT} + \frac{3 N_{impurity} \bar{v} \tau_{s0}}{2 d T'_i} e^{E_{ad}/kT} \quad (1.11)$$

According to the above equation, both the diffusion-induced and the surface-induced relaxation rates are proportional to the surface-volume ratio of the cell, *i.e.* to the inverse of the cell diameter d . Thus it is useful to describe the surface relaxation properties with a physical quantity ρ , which is commonly referred to as the “relaxivity”. The relaxivity is independent of cell geometry and is related to the wall relaxation rate $1/T_{wall}$, the surface to volume ratio A/V by the following equation:

$$1/T_{wall} = \rho A/V \quad (1.12)$$

Fitzsimmons *et al.* [31] found by using impermeable aluminosilicate glass, the relaxation due to absorption can be greatly reduced thus increasing the total relaxation time. Heil *et al.* reported [36] glass cells that were internally coated with metallic films provided even longer relaxation time. Cs was one of the metals that greatly reduced wall relaxation rate as it blocks ^3He atoms from diffusing into the glass walls and it also has a low adsorption energy which leads to very short sticking time. For SEOP (Spin-Exchange Optical Pumping), we automatically profit from the Rb film which covers the inner surface of the pumping chamber. Similarly, another way to eliminate relaxation due to absorption is to coat the inner surface with sol-gel [38]. It is a mixture of aluminum nitrate nonahydrate $Al(NO_3)_3 \cdot 9H_2O$, ethanol and deionized water. The sol-gel coating also improves relaxation time by blocking ^3He atoms from diffusing into the glass.

1.2.2 Relaxation on Metal Surfaces

Since ^3He gas does not diffuse into metals [14], the relaxation is purely due to surface effects. However, the surface-induced relaxation on metal surfaces is not yet well understood. There are two additional relaxation mechanisms that need to be considered with metal surfaces compared to those for glass. The first mechanism is the depolarization of ^3He nuclei near the metal surface by oscillating magnetic field from eddy currents induced by the movement of these same nuclear dipoles. Smythe [59] derived the magnetic field generated by eddy current induced in a metal sheet by a moving magnetic dipole using the method of images. Timsit *et al.* [1] estimated the relaxation due to eddy currents using the same method:

$$\frac{1}{T_m} = \frac{3 \times 10^{-4}}{\pi} \frac{\mu_{He}^4}{\bar{v} r_0^4 \hbar^2} \frac{A_p}{d^3} \quad (1.13)$$

where \bar{v} is the mean velocity of atoms, r_0 is the closest distance of the nucleus to the metal surface, d is the cell diameter, A_p is the area. According to Timsit *et al.* [1], T_m is on the order of 10^{16} s if $r_0 = 1\text{\AA}$ and $A_p = 9.2\text{cm}^2$. Even though the area of the cell is usually much larger in our studies and other parameters may take different values, it should still remain true that the relaxation rate of ^3He due to eddy currents can be safely neglected.

The second additional mechanism that contributes to relaxation of ^3He adsorbed on the metal surfaces is Korringa scattering [42]. Nuclear spins relax when the nuclei interact with conduction electrons in the metal, where the electrons flip spins and the spin states of the nuclei change. The Pauli exclusion principle states that the interaction is only allowed when the final state the electrons jump to are initially unoccupied. Thus according to Fermi statistics, only electrons with energy close (ap-

proximately within kT) to the Fermi energy level can participate in such interactions.

Slichter [58] has derived the Korringa relaxation rate in metal to be:

$$\frac{1}{T_K} = \frac{(4\pi)^6}{9h^7} (g_s\mu_B \frac{\mu_K}{K})^2 \eta^4 m^3 \epsilon_F k T \quad (1.14)$$

To calculate the total Korringa relaxation rate due to a metal surface, one needs to consider the overlapping of wave functions of the conduction electrons and the nuclei of adsorbed ${}^3\text{He}$ atoms in the vicinity of the metal surface. Nelson [2] derived the total surface Korringa relaxation as:

$$\frac{1}{T} = \frac{1}{T_K} \frac{S}{V} \int_0^\infty f(l)^2 e^{-U(l)/kT} dl \quad (1.15)$$

where S and V are the surface area of the metal and total volume of the cell, respectively, $U(l)$ is the atom-surface potential with the edge of the metal taken as $l = 0$, $f(l)$ is the fractional density of conduction electrons outside the surface. Nelson further used the work function of the metal to estimate $f(l)$, and assumed a van der Waals form for $U(l)$. His calculations suggest that the Korringa relaxation times for ${}^3\text{He}$ on various metal surfaces should be thousands of years, including the metal of interest for our studies, gold.

If eddy currents and Korringa relaxation are the only surface relaxation mechanisms, we would have very long lifetime for our test metal cells. Unfortunately, our series of studies have shown relaxation times to be between a few hours and 16 hours most of the time, for which both aforementioned relaxation mechanisms can be safely neglected. Although the dominating relaxation mechanism is still not well understood and significantly faster than those for which we have a better understanding, the results of our studies are still promising, as they suggest that the extra relaxation

rate due to the use of metal end windows should still be small enough to allow future experiments to run at $60\mu\text{A}$ electron beam current.

1.3 Test Cell Fabrication

1.3.1 Overview

In order to study the relaxation rate due to metal surfaces, we have created and tested 19 cells, most of which contained metal tubes. The metal tubes were 5" in length and had 1" outer diameter, 3" of glass tubes were attached to both ends via a Houskeeper seal [37]. The resulting glass-to-metal-to-glass assembly is shown in Fig. 1.1The total area of the metal surface was 101.3 cm^2 , and was far larger than what we anticipated would be used for metal end windows. This large geometry was chosen to intentionally increase the relaxation rate due to metal. This particular design for the metal tubes was also favored for the convenience of manufacturing, as we were expecting a large number of test cells to be studied and any design that could save time had the potential to lead to a much shorter test time before finding a final design. A finished cell in 1.1 will be discussed later.

The making of these test cells usually included five steps:

1. Larson Electronic Glass [34] provided us a glass-to-metal-to-glass tube that used Houskeeper seal to bond glass and metal together.
2. The machine shop in the Physics Department of University of Virginia then mechanically polished the inside of the metal tube.
3. Able[60] Electropolishing electropolished the metal tube.



Figure 1.1: Shown on the left is a glass-to-metal-to-glass seal. The metal tube is 5" long by 1" outer diameter. The glass is wetted onto the knife-edge of copper on both ends. Shown on the right is a finished cell with the glass-to-metal-to-glass tube attached.

4. Epner[40] Technology Inc. electroplated the metal tube with gold.
5. Mike Souza at Princeton University, our glass blower, resized glass from stock



Figure 1.2: Glass-to-metal seals survived pressure higher than 20 atm.

material and made the final cell incorporating both glass and metal components. The resizing was for removing micro-fissures from the glass surface and reducing wall relaxation rates [21].

Each step will be described in what follows.

1.3.2 Glass-Metal Seal

Larson Electronic Glass fabricated our glass-metal-glass tubes as shown in Fig. 1.1. The glass-to-metal seal used by Larson is known as a Houskeeper seal [37]. The outside of the copper tube is machined down to a knife edge and is wetted with glass. The edge of copper is usually heated before covering with glass. The heating process creates a thin layer of crimson-color copper oxide as can be seen in Fig. 1.1. Houskeeper seals were originally used for vacuum, and we checked each seal down to the level of $10^{-10}\text{mbar} \cdot \text{l/s}$. To make sure that these seals would survive the high pressure JLab experiments, we also tested the integrity of them at pressures up to 20 atm for extended period of time.

The copper used in our tests was OFHC (oxygen-free high thermal conductivity)

copper. In the earlier stage of our tests, OFHC copper was attached to Pyrex glass, in which case a direct connection could be made. For the later tests where we were moving closer to the final goal of using metal end windows with the impermeable aluminosilicate glass GE180, a transition glass between OFHC copper and GE180 had to be used. The coefficient of expansion for GE180 glass is not compatible for making a direct seal with OFHC copper, thus Corning 7052 Kovar sealing glass was used as the transition. The two materials connected by a seal should have similar coefficients of expansion, and the 7052 Kovar sealing glass served as an intermediate material to bridge the gap between OFHC copper and GE180. The other type of metal used in our glass–metal seals was titanium, for which only Pyrex was used.

1.3.3 Mechanical Polishing and Electropolishing

The mechanical polishing was done locally by our machine shop in the Physics Department. A wire brush attached to a lathe was placed inside the tube while the lathe spun. This first step of polishing produced a relatively smooth surface in preparation for the electropolishing process.

After the tubes were mechanically polished by the machine shop, they were sent to Able Inc. for electropolishing. The tube served as the cathode, which was immersed in a temperature-controlled bath of electrolyte and connected to the positive terminal of a DC power supply, while the cathode attached to the negative terminal. During electropolishing, the polarized film is subjected to combined effects of gassing (oxygen) that occurs with electrochemical metal removal, saturation of the surface with dissolved metal and the agitation and temperature of the electrolyte. Metal on

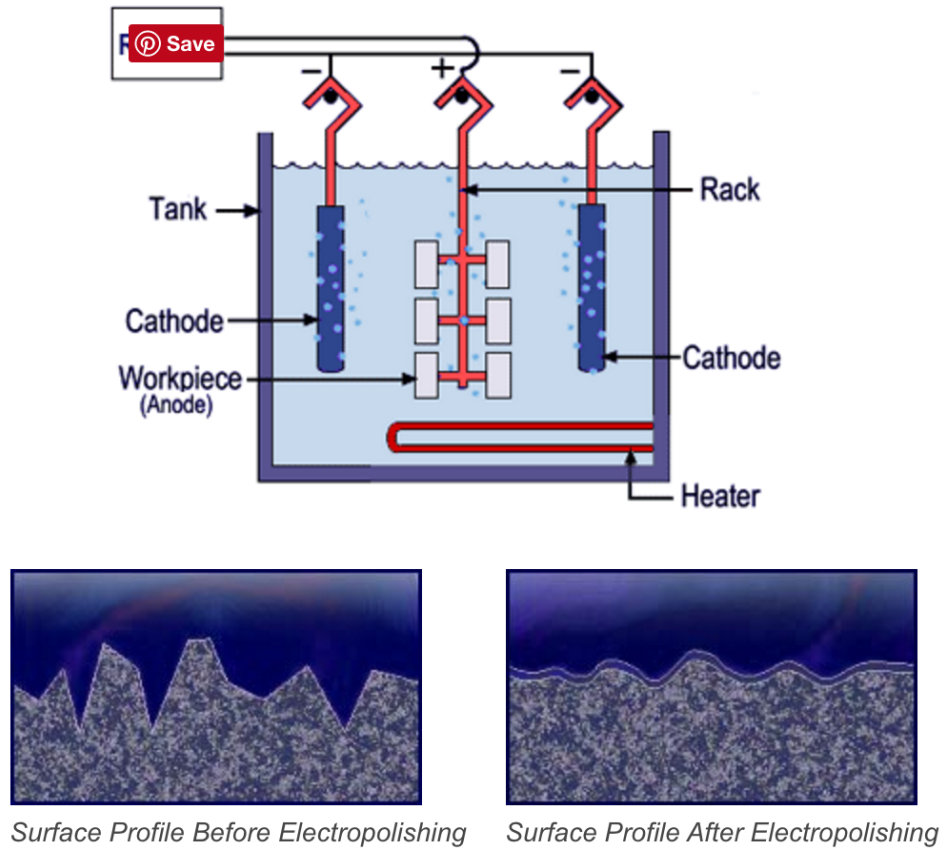


Figure 1.3: Electropolishing [28]

the surface is oxidized and dissolved in the electrolyte, the microscopic high points on the surface dissolve faster than the rate of attack on the other parts of the surface, which provides a smoothing effect. As a result, the electropolishing process removes a thin layer of metal (about $20 \mu\text{m}$ for our tubes), leaving a microscopically smooth and featureless surface. By contrast, even a fine mechanically polished surface will still show smears and other directionally oriented patterns or effects[28]. Fig. 1.3 shows a diagram of the polishing process and its smoothing effect.

1.3.4 Electroplating

As stated earlier, because of the good lifetime reported by Deninger *et al.*[29], gold was plated on the inner surface of the OFHC copper and titanium tubes. Epner Technology Inc. did the electroplating for us. Electroplating is the reverse process of electropolishing. When electric current passes through the electrolyte, the electrolyte splits up and some of the desired metal atoms it contains are deposited in a thin layer on top of the electrodes. Nickel and chromium are two common undercoatings used for electroplating, however, they are both ferromagnetic and cannot be used for us as they would introduce additional spin relaxation. As a result, Epner used a copper strike to improve the durability of gold coating. A $5 \mu\text{m}$ layer of gold was subsequently electroplated on the inner surface of the tubes. Fig.1.4 shows a comparison of an OFHC copper tube with and without gold-coating.

1.3.5 Final Assembly of the Cell

After the tubes were coated, shipped back to us and leak checked one more time, they were cleaned with our ultrasonic cleaner. Fig. 1.5 shows the setup of the cleaning process. We cleaned the impurities on the surfaces of the tubes with ethanol, deionized water and methanol for thirty minutes each. As shown in the figure, a beaker containing the chemical solution and the tubes were placed in water bath inside the ultrasonic cleaner. Because of the dimensions of the cleaner and the beaker, we cleaned one end of the tubes first then flipped them to clean the other end before switching solution.

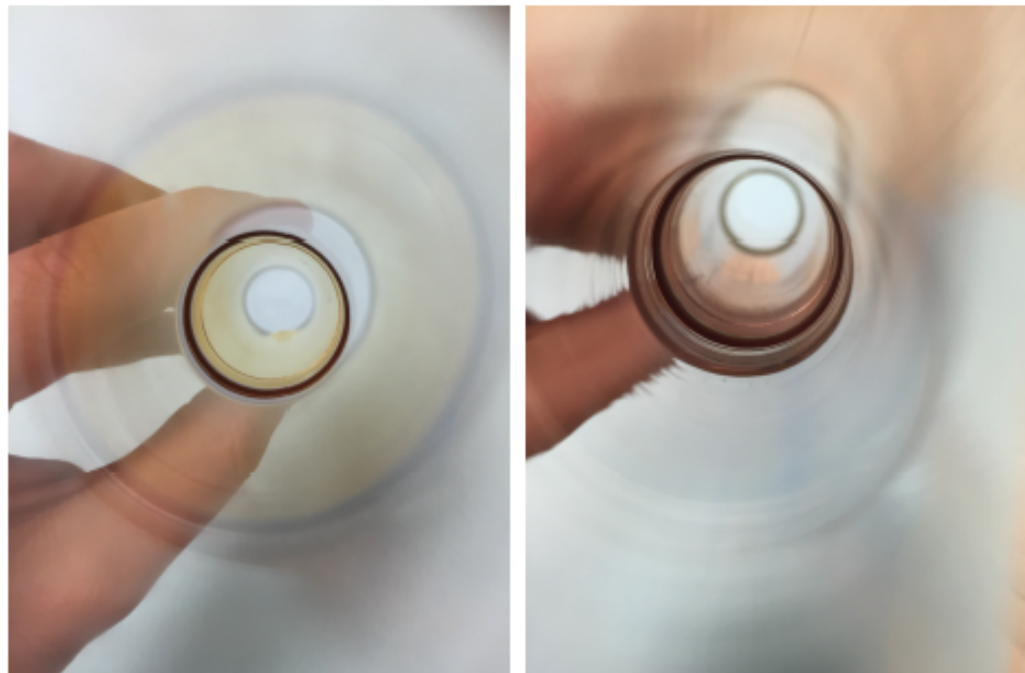


Figure 1.4: Shown left is the inner surface of a gold coated OFHC copper tube. Shown right is a OFHC copper tube without coating.



Figure 1.5: Ultrasonic cleaner with 3 tubes being cleaned.

The test tubes were then shipped to our glassblower Mike Souza at Princeton University. All glass was reblown to the right size to reduce micro-fissures which would lead to high relaxation rate. The test tube was spliced to transfer tube and pumping chamber as shown in Fig. 1.1. A string (see Fig. 1.6) which would be used for cell filling was also made at Princeton. Traditionally, a pure glass cell would be placed entirely in a oven for annealing. A cell made with GE180 would go through a five-minute ramping time to 780°C , stay at 780°C for five minutes and slowly cool down to room temperature for at least 5 hours [44]. A Pyrex cell would be annealed in the exact same way except the highest temperature is 565°C . However, most of our test cells could not have been annealed in the same way because of the glass-metal seal. Had we expose a seal to high temperature for long period of time, gold atoms might have migrated into the metal substrate and the seal might even break. Thus the metal tubes were attached to the rest of the glass parts after the pure glass parts were annealed.

1.4 Cell Fill Procedure

The details of cell fill was described thoroughly by Matyas [44], I will briefly cover the process for the sake of completeness.

1.4.1 Cell Fill Preparation

Although the actual cell fill work took less than a day, the preparation that led to the fill usually took 10-15 days. The glass manifold to which the cell was attached, the cell itself and a “retort” were spliced together and attached to our homemade gas

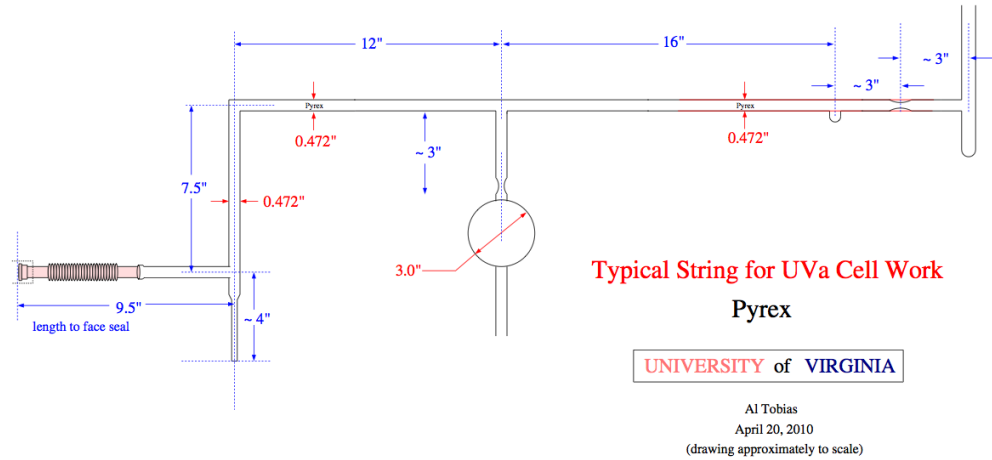


Figure 1.6: Shown is the design of a typical string for our test cells.

system through a bellows. A pre-scored ampoule of alkali metal was dropped into the top the of the retort. Fig. 1.7 is a diagram of the string, cell and retort all connected together.

The entire system was first rough-pumped with a mechanical pump, and then pumped by a diffusion pump to even higher vacuum. After the system was pumped for a few days and alkali metal was added in the system, we would keep pumping the system with the diffusion pump for roughly a week. To prevent back streaming of diffusion pump oil from getting into the gas system and the cell, a cold trap above the diffusion pump was filled every day with liquid nitrogen. “Flamebakes” were also performed 2-3 times each day during the one-week pumping period. A methane-oxygen torch was used to gently bake the glass during the flamebakes. The bake started from the retort which was the farthest away from the diffusion pump, and moved slowly towards the bellows, so the impurities chased off the inner surfaces

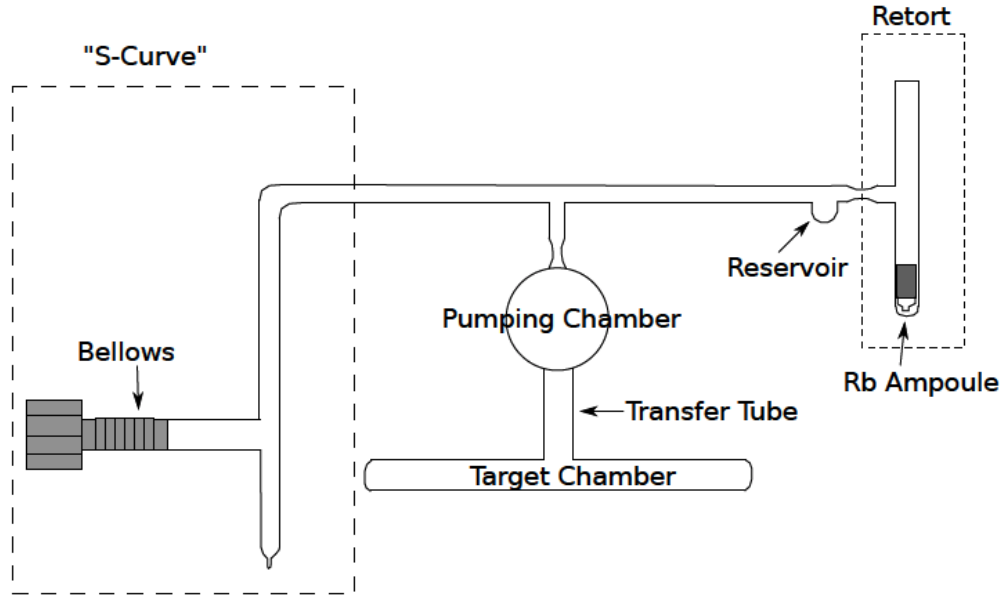


Figure 1.7: A diagram of a Pyrex string with a cell and a retort attached while connected to the gas system through the bellows. Adapted from Matyas [44].

could be “swept” towards the pump leaving as few impurities behind as possible. The alkali metal was typically melted in the retort starting with the second or third flamebake and continuing with each of the remaining flamebakes. On the day before the fill, alkali metal was melted and chased into the pumping chamber.

1.4.2 Cell Fill

The first thing on the fill day was to pump all portions of the gas system to vacuum and selectively back fill some parts with appropriate gases (either N₂ or ³He) to minimize outgassing. The gas filled into the cell should always be cleaned during the path to the cell. Earlier test cells were filled with the noble gas purifier while the

later cells were done with a homemade cryogenic trap.

The homemade cryogenic trap consisted of copper tubing placed inside a box-shaped Dewar. The Dewar was filled with liquid nitrogen when filling N₂ and liquid helium when filling ³He, so impurities in the gas were frozen in the copper tubing. Temperature inside the dewar was monitored with two silicon diodes to determine whether the copper tubing was fully submerged in the cold liquid.

The volume of the cell was also determined during the fill process. A Baratron pressure gauge was used to measure a calibrated volume (CV) of 992.9 cc. Roughly 300 Torr of gas was filled into the calibrated volume, then the valve on the CV was closed and any gas outside of CV was pumped away. Next the gas kept in the CV was let out into the fill gap between the CV and the string, then into the cell while monitoring pressure with the Baratron gauge, thus the volume of the cell could be calculated with the ideal gas law.

Around 70 Torr of nitrogen was put into the cell before filling with ³He. To prevent nitrogen from escaping the cell while filling ³He, the string valve was kept closed until ³He pressure in fill gap rose well above 70 Torr. A total gas pressure of just under 760 Torr (1 atm) was reached. The target pressure was chosen for practical reasons. When target cell was pulled off from the rest of the glass tubing, the connection between the cell and the string was melted. If the interior pressure was lower than 1 atm, the atmospheric pressure would essentially push the melted portion inward and seal the cell for us. The alkali metal used in filling all the cells described in this chapter was Rb, with the one exception of Kappa1 that was filled with a 5:1 mixture of K and Rb.

1.5 Experimental Setup and Procedure

All cells containing metal were tested with Pulse NMR in order to minimizes depolarization from eddy currents. Kappa1 was a simple spherical and pure GE180 cell, which was built to rule out the possibility that the melt of GE180 used in our cells had quality problems. Because of its lack of metal and lack of convenient places on which to wrap pickup coils, Adiabatic Fast Passage was used to test Kappa1. Both PNMR and AFP were discussed in a general way in chapter 3, I will only add to the discussions by describing more specific experimental setups used for these studies. Spindown measurements were the main means of studying relaxation properties, I will also discuss how we used spindowns with different sampling rate to extract PNMR losses and lifetime corrected for such losses.

1.5.1 Pickup Coils

In an AFP measurement, pickup coils are placed next to the side windows of the oven. However, the same setup proved to be more difficult for us to receive high-quality PNMR signals. To keep the pickup coils from the heat of the oven and to be physically close to the samples of ${}^3\text{He}$, we manually wrapped a solenoid coil on the transfer tube of test cells where it was approximately 2" below the bottom of the oven. These coils were made with 40-50 turns of AWG 20 copper wire. Because of the off-center position of the pickup coils with respect to the magnetic holding field, inhomogeneities were significant enough to affect FID signals, and gradient coils were used to cancel such inhomogeneities.

1.5.2 Gradient Coils

Inhomogeneities were minimized using three sets of gradient coils. Each set of gradients coils consisted of two oppositely wound coils separated by a distance d ; this particular type of coils is referred to as “Maxwell coils”. The setup is very similar to that of Helmholtz coils, except the opposite direction of currents and the larger optimum separation $d = \sqrt{3}R$, where R is the radius of the coils. The opposite direction is to cancel out the magnetic field at the center, and the optimum separation makes the nonlinear terms among the first four in the Taylor expansion of the inhomogeneities zero[20]. Fig.1.8 shows the coil orientations. The z axis is defined to be aligned with the direction of the holding field while x and y axes are in the transverse plane. The direction of coil axis is then defined by the angle θ and ϕ , where θ is with respect to the z axis and ϕ is the azimuthal angle in the x-y plane.

The magnetic field gradient at the center is given by[22]

$$\begin{aligned}\nabla \mathbf{B}(\theta, \phi) &= \begin{bmatrix} \partial B_x / \partial x & \partial B_y / \partial x & \partial B_z / \partial x \\ \partial B_x / \partial y & \partial B_y / \partial y & \partial B_z / \partial y \\ \partial B_x / \partial z & \partial B_y / \partial z & \partial B_z / \partial z \end{bmatrix} \\ &= 3\kappa I \begin{bmatrix} \sin^2 \theta \cos^2 \phi - \frac{1}{3} & \sin^2 \theta \sin \phi \cos \phi & \sin \theta \cos \theta \cos \phi \\ \sin^2 \theta \sin \phi \cos \phi & \sin^2 \theta \sin^2 \phi - \frac{1}{3} & \sin \theta \cos \theta \sin \phi \\ \sin \theta \cos \theta \cos \phi & \sin \theta \cos \theta \sin \phi & \cos^2 \theta - \frac{1}{3} \end{bmatrix} \quad (1.16)\end{aligned}$$

where the calibration constant κ is:

$$\kappa = \frac{3\pi n R^2 d / 2}{5(d^2/4 + R^2)^{5/2}} G \text{ cm A}^{-1} \quad (1.17)$$

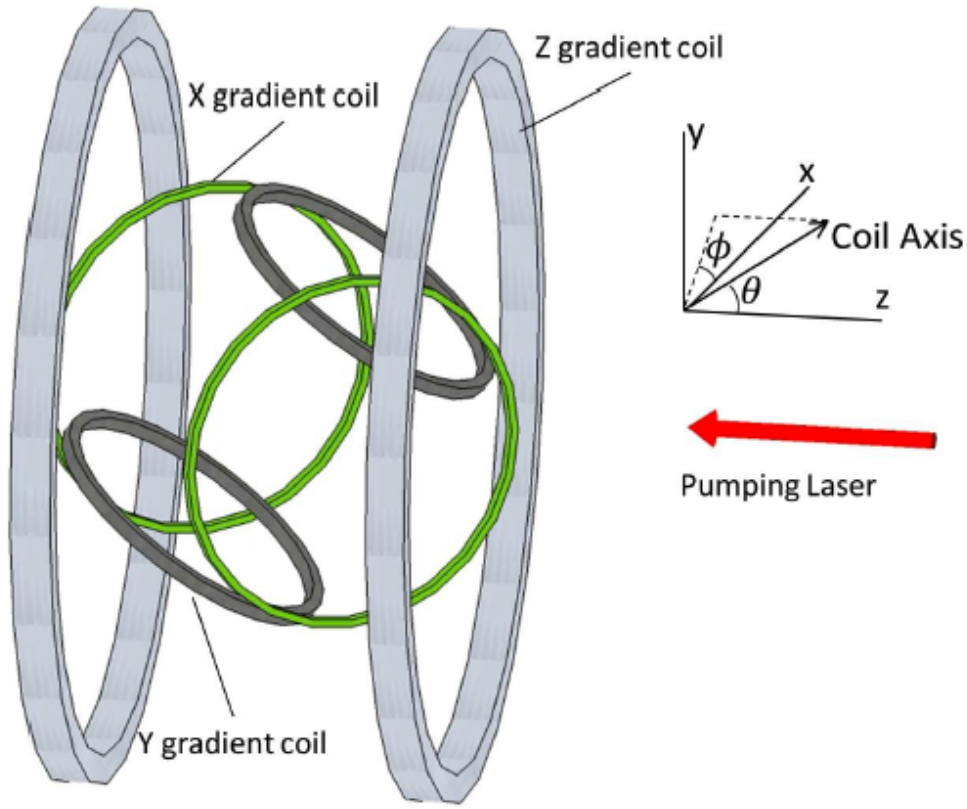


Figure 1.8: Diagram of the coils. Adapted from Zheng [68].

The most important terms in Eq.1.16 are those related to B_z : $\partial B_z / \partial x$, $\partial B_z / \partial y$ and $\partial B_z / \partial z$. The orientations of the gradient coils can be chosen such that each of the three sets of coils controls only one of the aforementioned terms. Such orientations require a specific value of θ which is referred to as the “magic angle” θ_m :

$$\theta_m = \cos^{-1} 1/\sqrt{3} = 54.7^\circ \quad (1.18)$$

For $\theta = \theta_m$ and $\phi = 0$ the gradient tensor is

$$\nabla \mathbf{B}(\theta_m, 0) = \kappa I \begin{bmatrix} 1 & 0 & \sqrt{2} \\ 0 & -1 & 0 \\ \sqrt{2} & 0 & 0 \end{bmatrix} \quad (1.19)$$

For $\theta = \theta_m$ and $\phi = \pi/2$ we have

$$\nabla \mathbf{B}(\theta_m, \pi/2) = \kappa I \begin{bmatrix} -1 & 0 & 0 \\ 0 & 1 & \sqrt{2} \\ 0 & \sqrt{2} & 0 \end{bmatrix} \quad (1.20)$$

Finally, for the z gradient coil we have

$$\nabla \mathbf{B}(0, 0) = \kappa I \begin{bmatrix} -1 & 0 & 0 \\ 0 & -1 & 0 \\ 0 & 0 & 2 \end{bmatrix} \quad (1.21)$$

Our gradient coils were built by Zheng [68]. The separations do not follow the optimum condition $d = \sqrt{3}R$ due to spatial limitations. The dimensions of the gradient coils are shown in Table 1.5.2.

	turns	radius	separation
x	42	33 cm	64 cm
y	100	28 cm	56 cm
z	8	66 cm	66 cm

1.5.3 Laser Setup

In an earlier stage of the study, narrow-band Comet lasers from Newport was used. Each Comet laser provided roughly 20 W power, the optical fibers were combined

through a “combiner” which required water cooling if multiple lasers were used at the same time. In later studies, a single Raytum laser was used instead as it could provide much higher power. Both the Comet laser and Raytum laser had around 0.2 nm FWHM (full width at half maximum).

Fig. 1.9 shows a diagram of the optics used for SEOP (spin-exchange optical pumping). After coming out of the fiber head, laser was focused by two lenses L1 and L2 such that the power spread enough to not damage the polarizing cube and was focused to an appropriate size at the cell position. The polarizing cube separated the beam into two beams with orthogonal linear polarizations. The beam with polarization parallel to the plane of the figure went through the cube, and the other beam with polarization perpendicular to the plane was reflected. The reflected beam went through a QWP (quarter wave plate), reflected at a mirror, went through the QWP one more time. Its polarization was changed to be parallel to this plane at this point and went through the cube. This beam is referred to as the “main beam” as it is ideally aligned with the holding field. The beam that went through the cube the first time was sent towards the oven by a mirror. Because of the small angle relative to the main beam, this is called the “skew beam”. Both the main beam and the skew beam went through QWP before arriving at the oven window and were turned to circular polarization in the same direction.

1.5.4 PNMR Losses and Corrected Lifetime

As described in chapter 3, there are generally two methods for us to determine polarization losses due to measurements: one is to take several measurements quickly

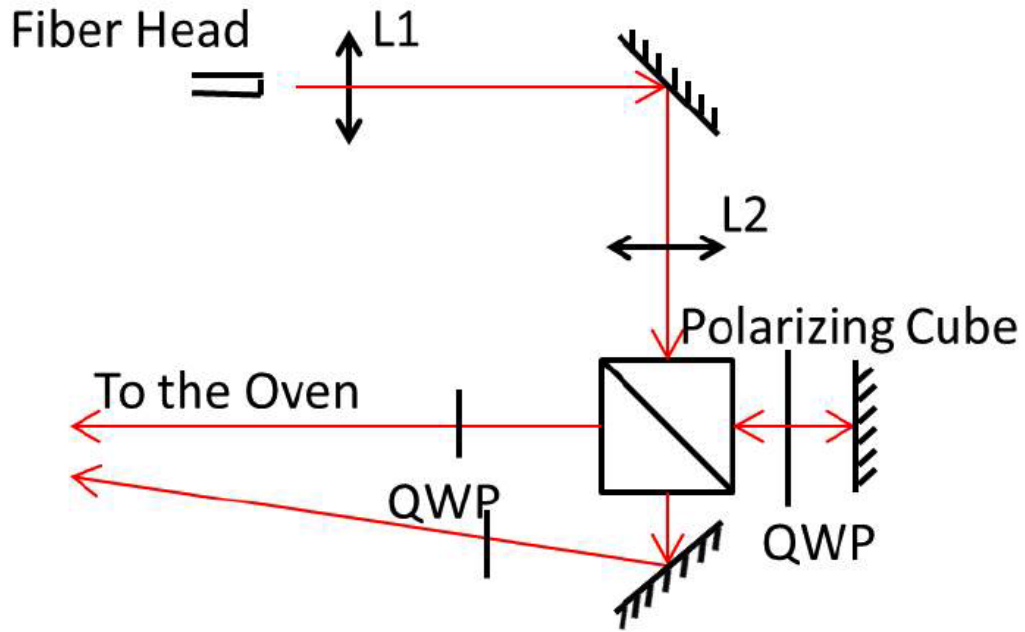


Figure 1.9: Optics for spin-exchange optical pumping. Adapted from Zheng [68].

enough that all depolarization can be attributed to measurement losses, the second method is to take multiple spindown measurements each with a different sampling rate. PNMR measurements cause a fraction of longitudinal polarization to be lost, two adjacent measurements require a long enough separation so the depolarization effect can be fully dispersed. For this reason, the first method mentioned above is not an option for PNMR. We have applied the second method to most of the 19 test cells that had lifetime of at least a few hours.

A spindown typically comprises a series of measurements of FID (Free Induction Decay) signals. Obtaining a good FID signal generally requires tuning the holding magnetic field and the gradient settings to reduce inhomogeneities.

In a PNMR measurement, it is important that the RF frequency is the correct Larmor frequency of the holding field. The RF frequency was set to be at 56.6 kHz, it

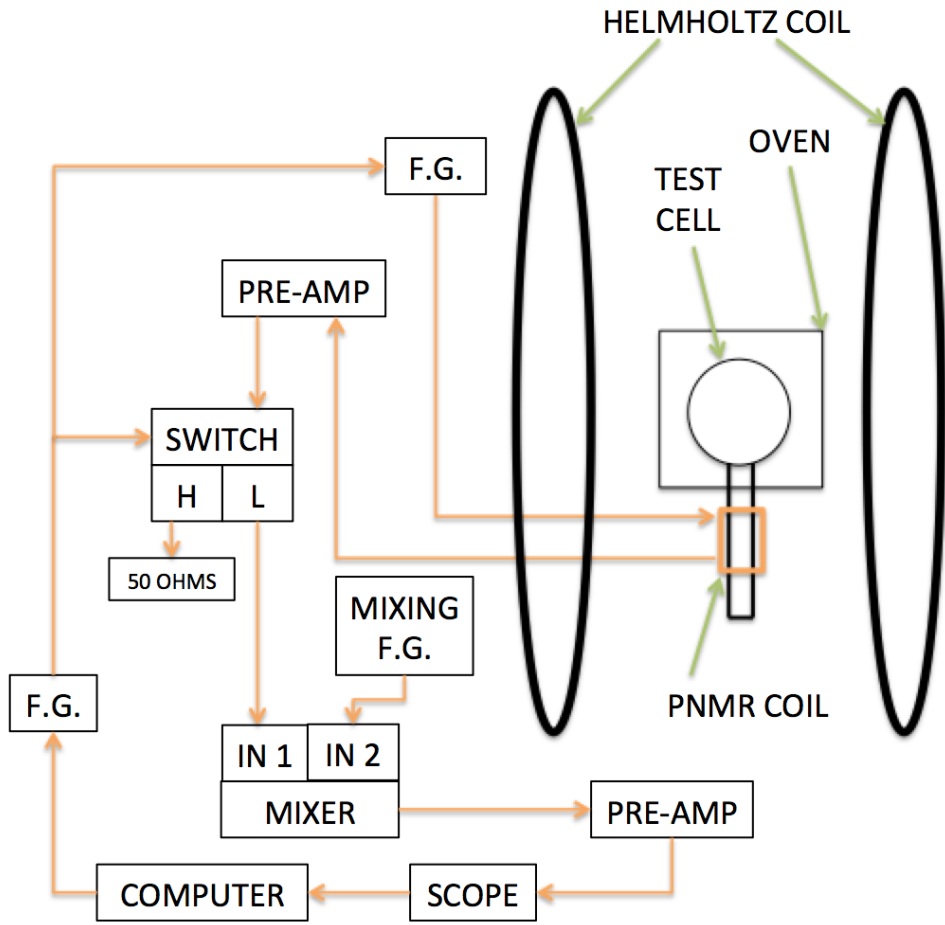


Figure 1.10: PNMR setup.

was often the case the holding field would start being off-resonance at the beginning. As Fig. 1.10 shows, the signal collected by the pickup coil was mixed with a mixing frequency before being recorded. The output of the mixing process gave us the a signal whose frequency was the absolute value of the difference between the signal frequency and the mixing frequency. By lowering the frequency from 56.6 kHz to below 100 Hz, we were able to use the band pass on the preamplifier to improve the signal to noise ratio. However, this lower frequency does not provide information about whether the

frequency of the signal (which was proportional to the holding field) was above (or below) the mixing frequency. By intentionally changing the mixing frequency by an appropriate amount and observing if the recorded frequency increased or decreased, we were able to tell whether the recorded frequency should be added to or subtracted from the mixing frequency to give us the true signal frequency. The holding field was proportional to the current which was monitored with a shunt resistor, thus the next step was to use the proportionality to calculate the corresponding shunt resistor value for the correct field for the RF pulse. This was further complicated by non-zero fields produced by gradient coils as the pickup coil location was not at the center of the coils. However, the calculation of shunt resistor value typically brought us closer to the resonance field.

The settings of the gradient coils also required tweaking in most cases. In order to reach longer transverse relaxation time T_2^* , the inhomogeneities needed to be low. Because the pickup coils were often at least 3-4 inches below the center of the fields, gradient coils were very useful for decreasing the inhomogeneities. The center of the pickup coils was in the same x-y plane (x, y and z axes were defined the same way as in Fig.1.8) with the center of the fields, so it was expected either $\partial B_z / \partial x$ or $\partial B_z / \partial y$ was initially the dominant term in field inhomogeneities. So x or y gradient coils should provide the most significant improvements at the beginning, while it also produced non-zero partial derivatives in other directions that needed to be canceled with other gradient coils later and non-zero field that required further field tuning. The adjusting of the holding field and the gradients settings were an iterative process for achieving long T_2^* and high-quality FID signals. Fig. 1.11 shows an FID signal with approximately 150 ms T_2^* . FID signal was typically fitted to the equation:

$$s(t) = a \sin(\omega t + \phi) e^{-t/T_2^*} + b \quad (1.22)$$

where a is the amplitude of the signal, b is the offset, ω is the RF frequency, ϕ is an offset of the phase and T_2^* is the measured transverse relaxation time. The amplitude a was used to represent the points in spindowns.

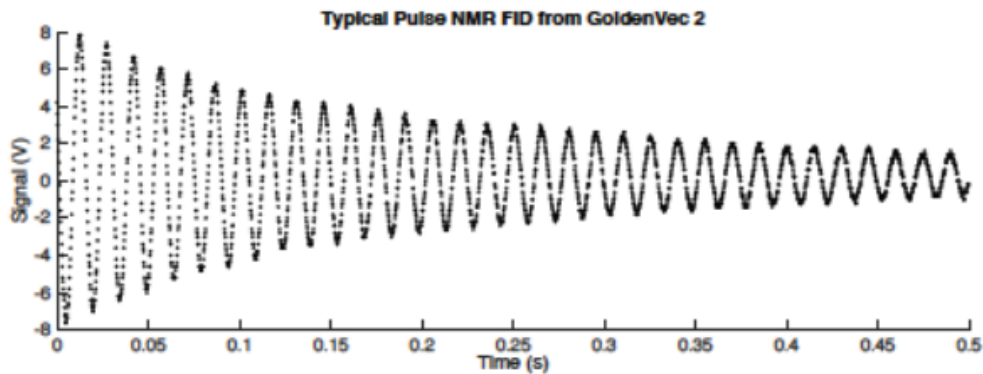


Figure 1.11: A PNMR signal taken with gold coated test cell.

Once the optimal settings were found, multiple spindowns were taken. Each spindown was a series of PNMR measurements set apart with a fixed time interval. Multiple values of intervals were used for different spindown measurements, each of the intervals was typically repeated at least twice. Fig. 1.12 shows 3 spindowns for the test cell GoldenVec1 which had a horizontal metal tube and similar configuration to that of a convection style cell. The time interval used for the 3 spindowns were 20 min, 30 min and 60 min, respectively. Using the additional relaxation rate due to taking PNMR once every hour as the base rate Γ_{PNMR} , the measured relaxation rate for taking n PNMR every hour can be related to the true lifetime (without relaxation

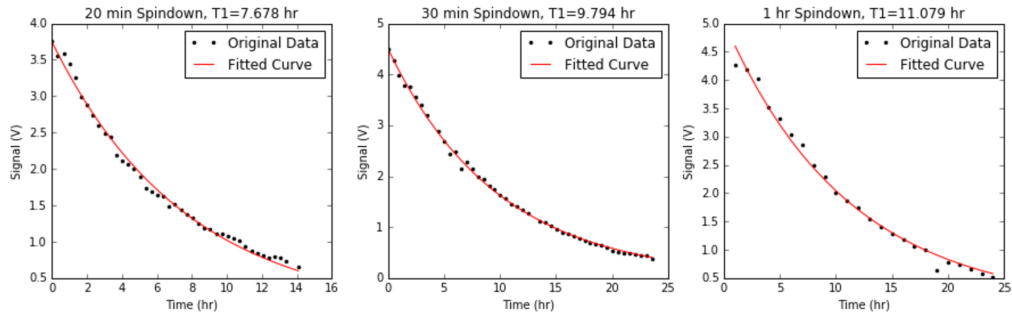


Figure 1.12: 3 spindowns of the cell GoldenVec1 each with a different sampling rate.

from PNMR) by:

$$\frac{1}{T_{measured}} = \frac{1}{T_{true}} + n \cdot \Gamma_{PNMR} \quad (1.23)$$

in the relation of $\frac{1}{T_{measured}}$ versus n , $\frac{1}{T_{true}}$ is the intercept, and the Γ_{PNMR} is the slope.

Fig. 1.13 shows the linear fit between the sampling rates (n) as x and the inverse of measured lifetimes as y . The intercept is 0.0676 hr^{-1} , thus the true lifetime without any loss due to taking PNMR measurements is $1/0.0676 = 14.8 \text{ hr}$. The slope is 0.02 hr^{-1} , which means the relaxation rate due to taking one PNMR per hour is $1/50 \text{ hr}^{-1}$. The percentage loss of polarization due to a single PNMR measurement can be calculated as:

$$1 - e^{-t \cdot \Gamma_{PNMR}} = 1 - e^{-1 \times \frac{1}{50}} = 0.0198 = 2\% \quad (1.24)$$

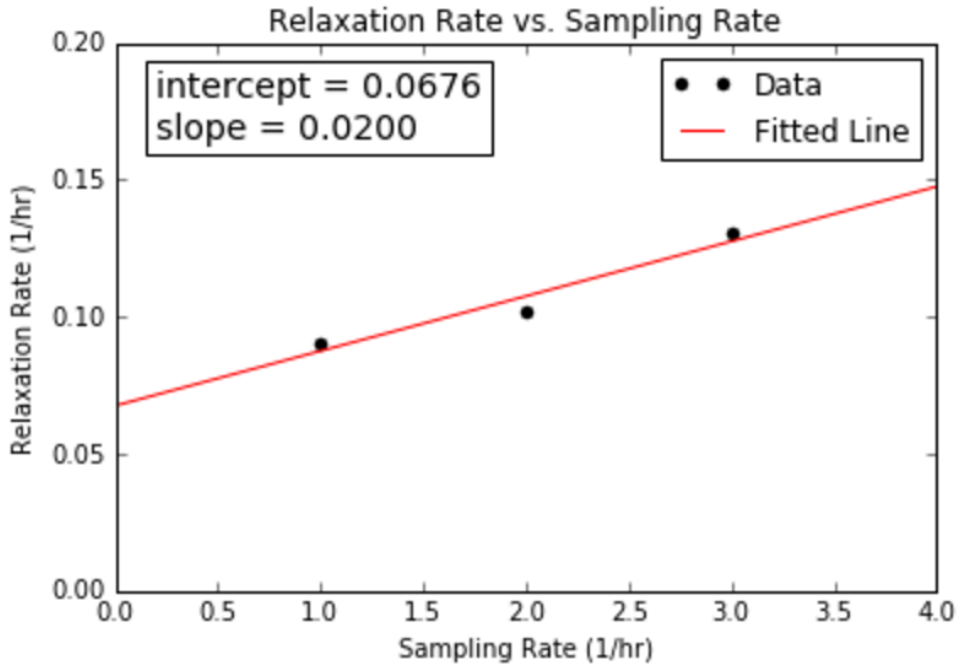


Figure 1.13: A linear fit to extract lifetime corrected for relaxation due to PNMR losses.

1.6 Relaxation Measurement Results and Discussion

The end goal of this series of studies was to replace the traditional glass end windows on our target chamber with metal end windows as Fig. 1.14 shows. Although no metal end windows have been produced yet, 19 test cells with various configurations and compositions were studied to explore the feasibility of incorporating metallic components into glass cells. We have gone through different stages of studies, and from each we made new discoveries and stepped closer to the end goal. At this point, we have demonstrated that gold coated OFHC copper is strong enough to survive the



Figure 1.14: A diagram of target cell with metal end windows.

high gas pressure of electron scattering experiments, only brings a relatively small amount of relaxation rates to a convection style target cell made with GE180 under SEOP conditions. The following discussion will be separated into different stages that each revealed parts of the mystery and generally follow chronological order (except cells made with titanium will be covered at the end). The cell preparation information and results of measurements are listed in Table 1.1.

1.6.1 Gold Coated Spherical Cell

Our very first attempt at incorporating metal was a spherical GE180 glass cell with gold coated on the interior surface. Although this attempt was made before I joined the group as were the spool pieces that will be mentioned below, they are still included for the sake of completeness of this study.

The measured lifetime of the first test cell was only 1.21 hr, which was attributed to impurities in the cell. Several attempts were made to identify better coating

Cell Name	Fill Type	Geometry	Glass	Metal	Max Lifetime (hr)	Fill Date
Tyrion	NGP	Sphere	GE180	Gold on glass	1.21	6/18/09
Gold Maiden1	NGP	Flange	Pyrex	Gold on Copper	2.14	6/18/10
Gold Maiden2	NGP	Flange	Pyrex	Gold on Copper	None	8/14/10
Gold Maiden3	NGP	Flange	Pyrex	Gold on Copper	6.49	11/11/10
Goldfinger	NGP	Vertical	Pyrex	Gold on Copper	3.59	4/28/13
Cupid	NGP	Vertical	Pyrex	Bare Copper	3.13	6/15/13
Goldeneye	NGP	Vertical with Valve	Pyrex	Gold on Copper	13.94	10/2/13
GoldRush	NGP	Vertical	Pyrex	Gold on Copper	14.81 [†]	11/8/13
Pyrah	NGP	Vertical	Pyrex	None	26.52 [†]	2/1/14
GoldenVec	NGP	Horizontal	Pyrex	Gold on Copper	10.6	10/18/14
TitanVec	NGP	Horizontal	Pyrex	Gold on Titanium	0.52	12/15/14
GoldenVec2	Cryogenic	Horizontal	Pyrex	Gold on Copper	15.6	2/14/15
Titan	NGP	Vertical	Pyrex	Bare Titanium	None	3/11/15
GoldenVec180	Cryogenic	Horizontal	GE180	Gold on Copper	4.43	6/17/15
GolderVec360	Cryogenic	Horizontal	GE180	Gold on Copper	3.01	7/11/15
Tweety	Cryogenic	Vertical	Pyrex	Canary Glass	22.7	9/22/15
Sylvester	Cryogenic	Horizontal	GE180	Canary Glass	6.39	11/20/15
Kappa1	Cryogenic	Sphere	GE180	None	72.17	2/6/16
Goldfinger180	Cryogenic	Vertical	GE180	Gold on Copper	12.4 †	5/19/16

Table 1.1: Shown are the fill information, design and maximum measured lifetime of the test cells. Fill type is the method used to clean the gas. [†] indicates the maximum lifetime was obtained at an elevated position. Although canary glass is not metal, it is listed in the column of metal for Tweety and Sylvester for the sake of keeping the structure of the table simple.



Figure 1.15: A picture of Gold Maiden, generally referred to as the “spool piece”.

techniques, but it was decided that developing a better technique would not be easy. Since these early attempts involved gold on glass, not gold not metal, it was decided to move directly to studying gold-coated metal components where it was established that commercial services were available.

1.6.2 Gold Coated Spool Pieces

The first cell with a gold coated (by Epner) OFHC copper tube was named “Gold Maiden” and made in 2010. Fig. 1.15 is a picture of the cell which was referred to as the “spool piece”. The bottom end of the cell was capped off, while the other end was attached to a glass flange. The flange was then connected to the transfer tube of the cell. The seal was made with o-rings.

The tests of Gold Maiden was divided into three stages. Initially it had a lifetime of

2.14 hr before discoloration of Rb was observed. Discoloration is typically a sign of Rb reacting with air, which indicated either a leak or significant amount of outgassing from the o-rings. To separate Rb from possible outgassing, the pumping chamber was pulled off via glassblowing. Measurements of the separated pumping chamber showed a lifetime of 109.2 hr after correcting for AFP losses. The rest of the cell was attached to a different pumping chamber in each of the two series of measurements that followed. The second series of measurements did yield any meaningful result due to a leak. The third series of measurements produced a lifetime of 6.49 hr. The spool piece encouraged further investigation into gold coated OFHC copper that could be attached to glass without o-rings.

1.6.3 Vertical Cells

Since o-rings were the primary suspects of the short lifetime for the spool piece, a method to seal copper directly to the glass was highly desirable. We started using the Houskeeper seal, and five cells were made at this stage: Goldfinger, Cupid, Goldrush, Goldeneye and Pyrah. All 5 cells were designed to have the same dimensions. Fig. 1.16 shows the design drawing and a picture of the cell Goldfinger. Goldrush was of the same design. The only difference for Cupid was that the OFHC copper was not coated. Pyrah was a pure Pyrex control cell.

The first cell tested, Goldfinger, had a maximum lifetime of 3.59 hr at the beginning of the test. However, subsequent tests showed noticeable degradation. Towards the end of testing Goldfinger, the lifetime was at a minimum of 2.36 hr. Cupid had a similar maximum lifetime of 3.13 hr initially. However, a rapid degradation of lifetime

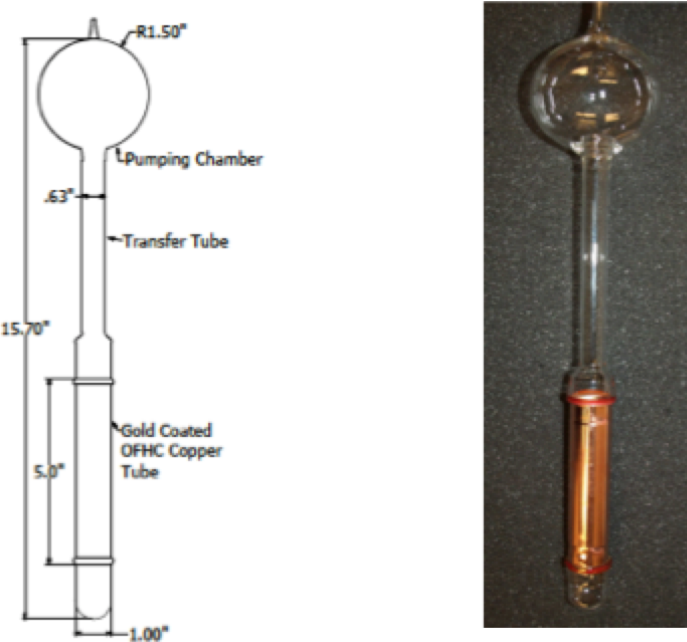


Figure 1.16: Design and picture of Goldfinger.

was observed. The last measurement we were able to perform displayed a lifetime of only 0.27 hr. It is worth noting a leak on Goldfinger was discovered during the filling process. Although the leak was fixed with Celvaseal Leak Sealant, either the sealant or the leak itself might have contributed to the short lifetime of Goldfinger and its degradation. The degradation could also be attributed to possible reaction between Rb and copper. Fig. 1.17 displays the lifetime degradation during our tests.

During the tests of Goldfinger and Cupid, it was suspected that Rb reacted with metal surfaces and produced detrimental effects to lifetime. A gold coated OFHC cell with a valve, GoldenEye, was designed and produced to isolate Rb vapor from the metal tube, as shown in Fig. 1.18. GoldenEye was only polarized with the valve closed, thus isolating the metal tube from most of the Rb vapor. Spindown

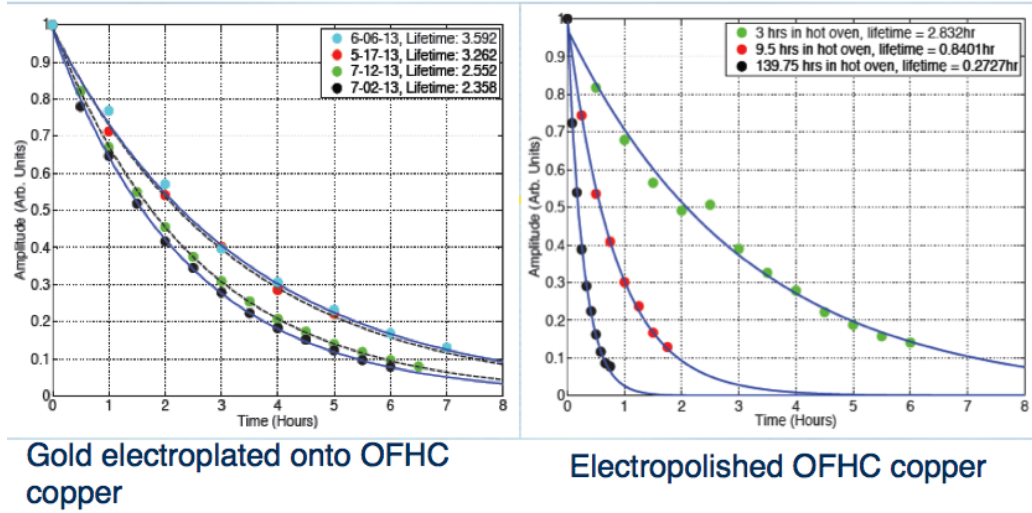


Figure 1.17: The observed degradation of lifetime for Goldfinger (left) and Cupid (right). Shown in each of the two plots were several spindowns at different stage during the tests. The initial amplitude of the spindowns were scaled to 1 for better comparison of lifetime.

measurements were taken at room temperature both with the valve closed and open. The lifetime was measured to be 13.94 hr with the valve closed, and it was only 4.09 hr with the valve open. The large difference of lifetime indicated the part of the cell below the valve introduced very significant relaxation rate. It is also worth noting the inclusion of the valve increased the total length of the cell substantially, which exposed the bottom part of the cell to high field inhomogeneities that could lead to high relaxation rate.

Due to the leak found in Goldfinger, it was necessary to produce another test cell with the same design, which was named as “Goldrush”. Fig. 1.19 displays four spindowns taken before tests in which the cell was elevated (will be discussed later). All four measurements have similar results with the maximum lifetime being 12.1 hr.



Figure 1.18: A picture of GoldenEye, the only test cell made with a valve.

This was the first metal cell we produced that had more than 10 hr lifetime.

A calculation of the magnetic field inhomogeneities was also done around the time. As seen in Fig. 1.20, the relaxation time due to inhomogeneities at the center of the pumping chamber was about 300-700 hr. However, the bottom of cell was exposed to surprisingly large inhomogeneities which would result in a relaxation time of 1-5 hr. This provided incentive for measurements of lifetime while raising the cell to more homogeneous region. Due to spatial constraints, the cell was only lifted by 10 cm, which led to an increase in lifetime to 14.81 hr, the longest lifetime we had measured at the time with metal cells.

To understand the additional relaxation rates introduced by metal surfaces, a control cell, Pyrah, was made with pure Pyrex was produced. The control cell had a lifetime of 19.71 hr before elevation, and 26.52 hr after being lifted by 10 cm.

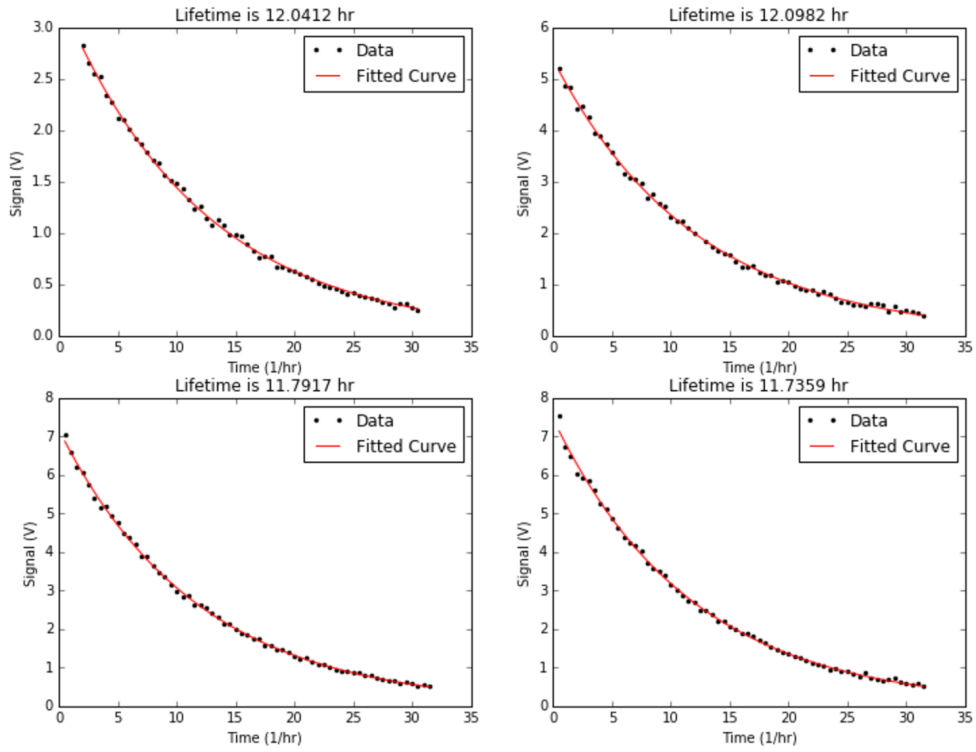


Figure 1.19: Four spindowns of Goldrush before elevating the cell. All four measurements display similar lifetime with no obvious sign of degradation.

Since Pyrah had the same dimensions as Goldrush, a direct comparison suggested the additional relaxation rate due to the metal tube was around $1/25\text{ hr}$.

1.6.4 Horizontal Cells

The increase of lifetime after elevating Goldrush and Pyrah motivated us to make more compact cell designs. This resulted in a design very similar to that of a convection style cells with the metal tube placed horizontally. The overall vertical length was shortened from 15.75" to about 10". The dimensions of this style of cells can be seen in Fig. 1.21.

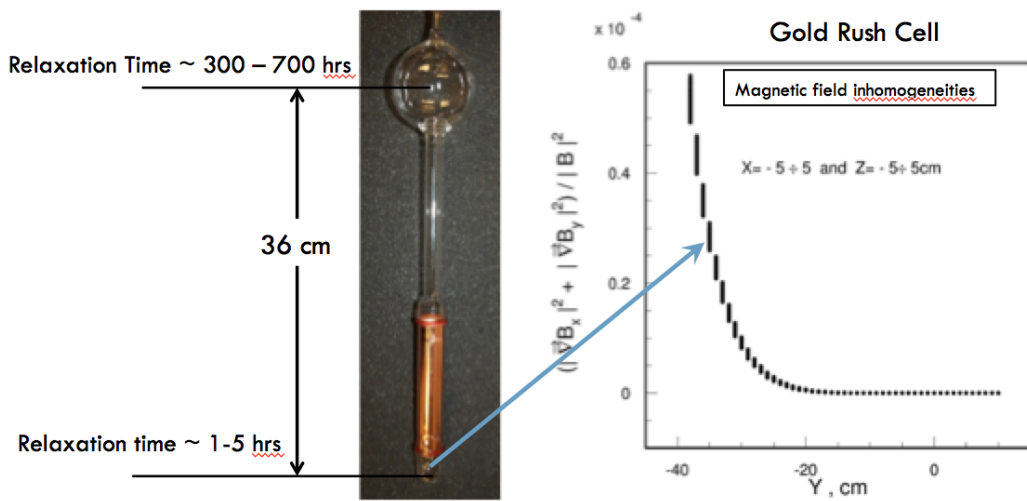


Figure 1.20: Shown on the right is the inhomogeneities vs. vertical distance from the center of the field. Shown on the left is the cell Goldrush with relaxation time due to field inhomogeneities as displayed on the right.

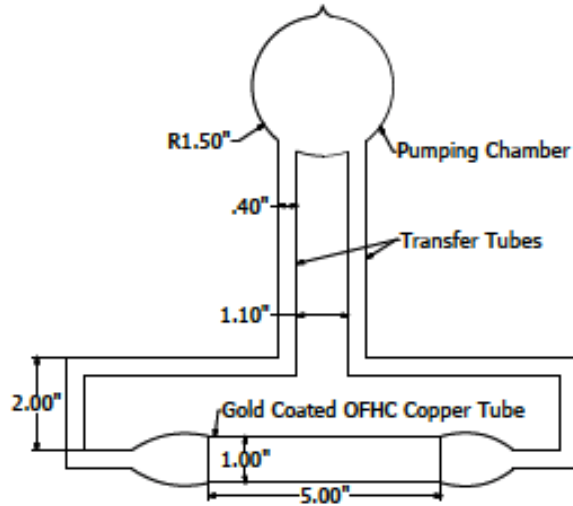


Figure 1.21: Design of the horizontal cell GoldenVec.

The first horizontal cell was GoldenVec. It had a lifetime of 10.6 hr, which was shorter than we had hoped for. Up to this point, all test cells were filled using

the noble gas purifier in our lab. A convection cell filled at the time that used the cryogenic trap to condense the impurities in the gas turned out to have much greater lifetime compared to the previous convection cell of the same design but used the noble gas purifier. In light of this, GoldenVec2 was created with the same design as that of GoldenVec and filled using a cryogenic trap. GoldenVec2's lifetime was measured to be 15.6 hr, the longest lifetime of metal cells we have obtained to date. All test cells from then on were filled using the same cryogenic trap.

1.6.5 GE180 Cells

It was widely acknowledged that the impermeable aluminosilicate glass GE180 had less associated wall relaxation rates than that of the borosilicate glass Pyrex. Since GoldenVec2 and Goldrush had demonstrated good enough lifetime, it was time we started exploring GE180 cells with metal tubes. Two GE180 test cells, GoldenVec180 and GoldenVec360, were made with the design as seen in Fig. 1.21. Because of the difficulty in bonding GE180 to OFHC copper, Corning 7052 was used as the transition glass. The measured lifetime of GoldenVec180 and GoldenVec360 were 4.43 hr and 3.01 hr, respectively. Since GE180 glass normally provide longer relaxation time, we made additional cells to test hypotheses to explain the short lifetime.

The first suspect occurred to us was the transition glass Corning 7052, since it had never been tested in our group. As we had experience with an alternative transition glass, canary glass (uranium glass), we built two test cells with 5" long by 1" OD tubes of the canary glass in place of copper tubes. The first was a replicate of the vertical cell Goldfinger and named as Tweety. The second was a replicate of the

horizontal cell GoldenVec and named as Sylvester.

Tweety had a lifetime of 22.7 hr, which was quite close to the lifetime of the control cell Pyrah, 26.52 hr. A shorter lifetime was expected as uranium is paramagnetic, however, the result of Tweety proved that that expectation was incorrect and canary glass could in fact be used to build target cell.

Sylvester was fabricated in the same way that GoldenVec was in that the canary glass tube and the GE180 portion directly connected to the tube were not annealed in a oven. The results of Sylvester were also unexpected as the lifetime was only 6.39 hr even in the absence of metal. This lifetime was shorter than that of GoldenVec and GoldenVec2. At this point, we narrowed down the causes of such short lifetime to the last two: 1. The melt of the GE180 glass had too much impurities. 2. Insufficient annealing resulted in more remaining micro-fissures in the glass.

The first possibility is easy to understand and could be easily tested with a simple spherical cell built from the same melt of GE180. Kappa1 was produced for this exact purpose. Hybrid Mixture of Rb and K was used instead of Rb because Kappa1 was also intended for future measurements of the physical quantity κ_0 which require hybrid mixtures. Kappa1 was found to have a lifetime of 72 hr, so the cause of high relaxation in previous GE180 cells was not the melt itself.

As mentioned in previous sections, to keep the glass-metal seals intact, all glass parts not directly attached to metal tubes were placed in a oven for annealing. Larger amount of micro-fissures could still exist in the glass directly attached to metal. This could potentially lead to the short lifetime we observed with the GE180 cells up to this point. To test the hypothesis, Goldfinger180 was built following the design of Goldfinger. However, the glass directly attached to the metal tube that did not

go into the oven was intentionally made shorter by our glassblower. During the fill process, a leak at the Houskeeper seal had to be fixed with two coats of an epoxy sealant Stycast 1266. The lifetime was measured to be 10.4 hr before elevation, and 12.4 hr after elevating in the same manner as Goldrush and Pyrah. The result both demonstrated the feasibility of using gold coated OFHC copper with GE180 and further confirmed the significance of glass annealing.

1.6.6 Titanium Tubes

Although gold coated OFHC copper was the main focus of the study due to the ease of manufacturing, titanium was also investigated for its stronger tensile strength. However, the results of the two titanium cells were not satisfactory. A test cell with bare titanium tube, Titan, had lifetime too short to be measured. The other cell TitanVec with gold coated titanium tube had lifetime of only 0.52 hr. Because of the difficulty in coating gold onto titanium surface, parts of gold coating peeled off the surface during the cleaning process with our ultrasonic cleaner. ^3He was exposed to part of the titanium surface underneath, which could be the reason for the bad relaxation properties. As a result, titanium was not investigated further.

Bibliography

- [1] Nuclear relaxation of ^3He gas on various solid surfaces. *Canadian Journal of Physics*, 1971.
- [2] Physics of practical spin-exchange optical pumping. *PhD thesis, University of Wisconsin-Madison*, 2001.
- [3] Spin-exchange optical pumping with alkali-metal vapors. *PhD thesis, University of Wisconsin-Madison*, 2005.
- [4] Alkali-hybrid spin-exchange optically-pumped polarized ^3He targets used for studying neutron structure. *PhD thesis, University of Virginia*, 2010.
- [5] High-performance nuclear-polarized ^3He targets for electron scattering based on spin-exchange optical pumping. *PhD thesis, University of Virginia*, 2010.
- [6] A. Abragam. *Principles of Nuclear Magnetism*.
- [7] M. S. Albert, G. D. Cates, B. Driehuys, W. Happer, B. Saam, C. S. Springer, and A. Wishnia. Biological magnetic resonance imaging using laser-polarized ^{129}Xe . *Nature*, 370.

- [8] M. Amarian, L. Auerbach, T. Averett, J. Berthot, P. Bertin, W. Bertozzi, T. Black, E. Brash, D. Brown, E. Burtin, J. R. Calarco, G. D. Cates, Z. Chai, J.-P. Chen, S. Choi, E. Chudakov, E. Cisbani, C. W. de Jager, A. Deur, R. DiSalvo, S. Dieterich, P. Djawotho, M. Finn, K. Fissum, H. Fonvieille, S. Frullani, H. Gao, J. Gao, F. Garibaldi, A. Gasparian, S. Gilad, R. Gilman, A. Glamazdin, C. Glashausser, E. Goldberg, J. Gomez, V. Gorbenko, J.-O. Hansen, F. W. Hersman, R. Holmes, G. M. Huber, E. W. Hughes, T. B. Humensky, S. Incerti, M. Iodice, S. Jensen, X. Jiang, C. Jones, G. M. Jones, M. Jones, C. Jutier, A. Ketikyan, I. Kominis, W. Korsch, K. Kramer, K. S. Kumar, G. Kumbartzki, M. Kuss, E. Lakuriqi, G. Laveissiere, J. Leroose, M. Liang, N. Liyanage, G. Lolos, S. Malov, J. Marroncle, K. McCormick, R. McKeown, Z.-E. Meziani, R. Michaels, J. Mitchell, Z. Papandreou, T. Pavlin, G. G. Petratos, D. Pripstein, D. Prout, R. Ransome, Y. Roblin, D. Rowntree, M. Rvachev, F. Sabatie, A. Saha, K. Slifer, P. A. Souder, T. Saito, S. Strauch, R. Suleiman, K. Takahashi, S. Teijiro, L. Todor, H. Tsubota, H. Ueno, G. Urchioli, R. Van der Meer, P. Vernin, H. Voskanian, B. Wojtsekhowski, F. Xiong, W. Xu, J.-C. Yang, B. Zhang, and P. Zolnierczuk. Q^2 evolution of the generalized gerasimov-drell-hearn integral for the neutron using a ${}^3\text{He}$ target. *Phys. Rev. Lett.*, 89:242301, Nov 2002.
- [9] P. L. Anthony, R. G. Arnold, H. R. Band, H. Borel, P. E. Bosted, V. Breton, G. D. Cates, T. E. Chupp, F. S. Dietrich, J. Dunne, R. Erbacher, J. Fellbaum, H. Fonvieille, R. Gearhart, R. Holmes, E. W. Hughes, J. R. Johnson, D. Kawall, C. Keppel, S. E. Kuhn, R. M. Lombard-Nelsen, J. Marroncle, T. Maruyama, W. Meyer, Z.-E. Meziani, H. Middleton, J. Morgenstern, N. R. Newbury, G. G.

Petratos, R. Pitthan, R. Prepost, Y. Roblin, S. E. Rock, S. H. Rokni, G. Shapiro, T. Smith, P. A. Souder, M. Spengos, F. Staley, L. M. Stuart, Z. M. Szalata, Y. Terrien, A. K. Thompson, J. L. White, M. Woods, J. Xu, C. C. Young, and G. Zapalac. Determination of the neutron spin structure function. *Phys. Rev. Lett.*, 71:959–962, Aug 1993.

- [10] S. Appelt, A. B.-A. Baranga, C. J. Erickson, M. V. Romalis, A. R. Young, and W. Happer. Theory of spin-exchange optical pumping of ^3He and ^{129}Xe . *Phys. Rev. A*, 58:1412–1439, Aug 1998.
- [11] E. Babcock, B. Chann, T. G. Walker, W. C. Chen, and T. R. Gentile. Limits to the polarization for spin-exchange optical pumping of ^3He . *Phys. Rev. Lett.*, 96:083003, Mar 2006.
- [12] E. Babcock, I. Nelson, S. Kadlecak, B. Driehuys, L. W. Anderson, F. W. Hersman, and T. G. Walker. Hybrid spin-exchange optical pumping of ^3He . *Phys. Rev. Lett.*, 91:123003, Sep 2003.
- [13] E. Babcock, I. A. Nelson, S. Kadlecak, and T. G. Walker. ^3He polarization-dependent epr frequency shifts of alkali-metal- ^3He pairs. *Phys. Rev. A*, 71:013414, Jan 2005.
- [14] R. M. Barrer. *Diffusion in and through Solids*.
- [15] A. Ben-Amar Baranga, S. Appelt, M. V. Romalis, C. J. Erickson, A. R. Young, G. D. Cates, and W. Happer. Polarization of ^3He by spin exchange with optically pumped rb and k vapors. *Phys. Rev. Lett.*, 80:2801–2804, Mar 1998.

- [16] F. Bloch. Nuclear induction. *Phys. Rev.*, 70:460–474, Oct 1946.
- [17] M. A. Bouchiat, T. R. Carver, and C. M. Varnum. Nuclear polarization in he^3 gas induced by optical pumping and dipolar exchange. *Phys. Rev. Lett.*, 5:373–375, Oct 1960.
- [18] G. Breit and I. I. Rabi. Measurement of nuclear spin. *Phys. Rev.*, 38:2082–2083, Dec 1931.
- [19] A. C., V. Itkin, and H. M.K. *Candadian Metallurgial Quarterly*, 23, 1984.
- [20] P. Callaghan. *Principles of Nuclear Magnetic Resonance Microscopy*.
- [21] G. D. Cates. Polarized targets in high energy physics. *Proceedings of the 1993 Summer Institute on Particle Physics: Spin Structure in High Energy Processes (SSI93)*, SLAC-R-444:185–207, 1993.
- [22] G. D. Cates, S. R. Schaefer, and W. Happer. Relaxation of spins due to field inhomogeneities in gaseous samples at low magnetic fields and low pressures. *Phys. Rev. A*, 37:2877–2885, Apr 1988.
- [23] G. D. Cates, D. J. White, T.-R. Chien, S. R. Schaefer, and W. Happer. Spin relaxation in gases due to inhomogeneous static and oscillating magnetic fields. *Phys. Rev. A*, 38:5092–5106, Nov 1988.
- [24] B. Chann, E. Babcock, L. Anderson, T. Walker, W. Chen, T. Smith, A. Thompson, and T. Gentile. Production of highly polarized ${}^3\text{he}$ using spectrally narrowed diode laser array bars. *Journal of applied physcis*, 94:6908–6914.

- [25] B. Chann, E. Babcock, L. W. Anderson, and T. G. Walker. Measurements of ^3He spin-exchange rates. *Phys. Rev. A*, 66:032703, Sep 2002.
- [26] T. E. Chupp, M. E. Wagshul, K. P. Coulter, A. B. McDonald, and W. Happer. Polarized, high-density, gaseous ^3He targets. *Phys. Rev. C*, 36:2244–2251, Dec 1987.
- [27] F. D. Colegrove, L. D. Schearer, and G. K. Walters. Polarization of he^3 gas by optical pumping. *Phys. Rev.*, 132:2561–2572, Dec 1963.
- [28] I. Delstar Metal Finishing. <https://www.delstar.com/electropolishing>.
- [29] A. Deninger, W. Heil, W. E. Otten, M. Wolf, K. R. Kremer, and A. Simon. Paramagnetic relaxation of spin polarized ^3He at coated glass walls. *The European Physical Journal D - Atomic, Molecular, Optical and Plasma Physics*, 38(3):439–443, 2006.
- [30] P. A. M. Dolph, J. Singh, T. Averett, A. Kelleher, K. E. Mooney, V. Nelyubin, W. A. Tobias, B. Wojtsekowski, and G. D. Cates. Gas dynamics in high-luminosity polarized ^3He targets using diffusion and convection. *Phys. Rev. C*, 84:065201, Dec 2011.
- [31] W. A. Fitzsimmons, L. L. Tankersley, and G. K. Walters. Nature of surface-induced nuclear-spin relaxation of gaseous ^3He . *Phys. Rev.*, 179:156–165, Mar 1969.
- [32] J. Frenkel. *Kinetic Theory of Liquids*.

- [33] R. L. Gamblin and T. R. Carver. Polarization and relaxation processes in he^3 gas. *Phys. Rev.*, 138:A946–A960, May 1965.
- [34] L. E. Glass. <http://www.larsonelectronicglass.com>.
- [35] W. Happer, G. Cates, M. Romalis, and C. Erickson. U.s. patent no. 6318092. 2001.
- [36] W. Heil, H. Humboldt, E. Otten, M. Schafer, R. Sarkau, and M. Leduc. Very long nuclear relaxation times of spin-polarized ${}^3\text{he}$ in metal coated cells. *Phys. Rev. A*, 201:337–343, May 1995.
- [37] W. G. Houskeeper. The art of sealing base metals through glass. *Transactions of the American Institute of Electrical Engineers*, XLII:870–877, 1923.
- [38] M. F. Hsu, G. D. Cates, I. Kominis, I. A. Aksay, and D. M. Dabbs. Sol-gel coated glass cells for spin-exchange polarized ${}^3\text{He}$. *Applied Physics Letters*, 77(13):2069–2071, 2000.
- [39] M. G. Huber, M. Arif, T. C. Black, W. C. Chen, T. R. Gentile, D. S. Hussey, D. A. Pushin, F. E. Wietfeldt, and L. Yang. Precision measurement of the $n-{}^3\text{He}$ incoherent scattering length using neutron interferometry. 102, 2009.
- [40] E. T. Inc. <http://www.epner.com>.
- [41] J. Jackson. *Classical Electrodynamics*.
- [42] J. Korringa. Nuclear magnetic relaxation and resonance line shift in metals. *Physica*, 16, 1950.

- [43] B. Larson, O. Hausser, P. P. J. Delheij, D. M. Whittal, and D. Thiessen. Optical pumping of rb in the presence of high-pressure ${}^3\text{He}$ buffer gas. *Phys. Rev. A*, 44:3108–3118, Sep 1991.
- [44] D. Matyas. Characterizing ${}^3\text{He}$ nuclear spin relaxation in vessels of glass and metal. *Master thesis, University of Virginia*, 2016.
- [45] E. Merzbacher. *Quantum Mechanics*. 1998.
- [46] N. R. Newbury, A. S. Barton, P. Bogorad, G. D. Cates, M. Gatzke, B. Saam, L. Han, R. Holmes, P. A. Souder, J. Xu, and D. Benton. Laser polarized muonic helium. *Phys. Rev. Lett.*, 67:3219–3222, Dec 1991.
- [47] N. R. Newbury, A. S. Barton, G. D. Cates, W. Happer, and H. Middleton. Gaseous ${}^3-{}^3\text{He}$ magnetic dipolar spin relaxation. *Phys. Rev. A*, 48:4411–4420, Dec 1993.
- [48] X. Qian, K. Allada, C. Dutta, J. Huang, J. Katich, Y. Wang, Y. Zhang, K. Aniol, J. R. M. Annand, T. Averett, F. Benmokhtar, W. Bertozzi, P. C. Bradshaw, P. Bosted, A. Camsonne, M. Canan, G. D. Cates, C. Chen, J.-P. Chen, W. Chen, K. Chirapatpimol, E. Chudakov, E. Cisbani, J. C. Cornejo, F. Cusanno, M. M. Dalton, W. Deconinck, C. W. de Jager, R. De Leo, X. Deng, A. Deur, H. Ding, P. A. M. Dolph, D. Dutta, L. El Fassi, S. Frullani, H. Gao, F. Garibaldi, D. Gaskell, S. Gilad, R. Gilman, O. Glamazdin, S. Golge, L. Guo, D. Hamilton, O. Hansen, D. W. Higinbotham, T. Holmstrom, M. Huang, H. F. Ibrahim, M. Iodice, X. Jiang, G. Jin, M. K. Jones, A. Kelleher, W. Kim, A. Kolarkar, W. Korsch, J. J. LeRose, X. Li, Y. Li, R. Lindgren, N. Liyanage, E. Long, H.-J.

Lu, D. J. Margaziotis, P. Markowitz, S. Marrone, D. McNulty, Z.-E. Meziani, R. Michaels, B. Moffit, C. Muñoz Camacho, S. Nanda, A. Narayan, V. Nelyubin, B. Norum, Y. Oh, M. Osipenko, D. Parno, J. C. Peng, S. K. Phillips, M. Posik, A. J. R. Puckett, Y. Qiang, A. Rakhman, R. D. Ransome, S. Riordan, A. Saha, B. Sawatzky, E. Schulte, A. Shahinyan, M. H. Shabestari, S. Širca, S. Stepanyan, R. Subedi, V. Sulkosky, L.-G. Tang, A. Tobias, G. M. Urciuoli, I. Vilardi, K. Wang, B. Wojtsekowski, X. Yan, H. Yao, Y. Ye, Z. Ye, L. Yuan, X. Zhan, Y.-W. Zhang, B. Zhao, X. Zheng, L. Zhu, X. Zhu, and X. Zong. Single spin asymmetries in charged pion production from semi-inclusive deep inelastic scattering on a transversely polarized ${}^3\text{He}$ target at $Q^2 = 1.4 \sim 2.7$ gev^2 . *Phys. Rev. Lett.*, 107:072003, Aug 2011.

- [49] I. I. Rabi, N. F. Ramsey, and J. Schwinger. Use of rotating coordinates in magnetic resonance problems. *Rev. Mod. Phys.*, 26:167–171, Apr 1954.
- [50] M. L. R. Barbe and F. Laloe. Experimental verifications - measurement of the ${}^3\text{He}$ self-diffusion coefficient. 35:935–951, 1974.
- [51] S. Riordan, S. Abrahamyan, B. Craver, A. Kelleher, A. Kolarkar, J. Miller, G. D. Cates, N. Liyanage, B. Wojtsekowski, A. Acha, K. Allada, B. Anderson, K. A. Aniol, J. R. M. Annand, J. Arrington, T. Averett, A. Beck, M. Bellis, W. Boeglin, H. Breuer, J. R. Calarco, A. Camsonne, J. P. Chen, E. Chudakov, L. Coman, B. Crowe, F. Cusanno, D. Day, P. Degtyarenko, P. A. M. Dolph, C. Dutta, C. Ferdi, C. Fernández-Ramírez, R. Feuerbach, L. M. Fraile, G. Franklin, S. Frullani, S. Fuchs, F. Garibaldi, N. Gevorgyan, R. Gilman, A. Glamazdin, J. Gomez, K. Grimm, J.-O. Hansen, J. L. Herraiz, D. W. Higin-

botham, R. Holmes, T. Holmstrom, D. Howell, C. W. de Jager, X. Jiang, M. K. Jones, J. Katich, L. J. Kaufman, M. Khandaker, J. J. Kelly, D. Kiselev, W. Korsch, J. LeRose, R. Lindgren, P. Markowitz, D. J. Margaziotis, S. M.-T. Beck, S. Mayilyan, K. McCormick, Z.-E. Meziani, R. Michaels, B. Moffit, S. Nanda, V. Nelyubin, T. Ngo, D. M. Nikolenko, B. Norum, L. Pentchev, C. F. Perdrisat, E. Piasetzky, R. Pomatsalyuk, D. Protopopescu, A. J. R. Puckett, V. A. Punjabi, X. Qian, Y. Qiang, B. Quinn, I. Racheck, R. D. Ransome, P. E. Reimer, B. Reitz, J. Roche, G. Ron, O. Rondon, G. Rosner, A. Saha, M. M. Sargsian, B. Sawatzky, J. Segal, M. Shabestari, A. Shahinyan, Y. Shestakov, J. Singh, S. Širca, P. Souder, S. Stepanyan, V. Stibunov, V. Sulkosky, S. Tajima, W. A. Tobias, J. M. Udiás, G. M. Urciuoli, B. Vlahovic, H. Voskanyan, K. Wang, F. R. Wesselmann, J. R. Vignote, S. A. Wood, J. Wright, H. Yao, and X. Zhu. Measurements of the electric form factor of the neutron up to $Q^2 = 3.4$ gev^2 using the reaction ${}^3\text{he} \xrightarrow{\vec{e}, e'n} pp$. *Phys. Rev. Lett.*, 105:262302, Dec 2010.

- [52] M. V. Romalis and G. D. Cates. Accurate ${}^3\text{He}$ polarimetry using the rb zee-man frequency shift due to the Rb– ${}^3\text{He}$ spin-exchange collisions. *Phys. Rev. A*, 58:3004–3011, Oct 1998.
- [53] M. V. Romalis, E. Miron, and G. D. Cates. Pressure broadening of rb d_1 and d_2 lines by ${}^3\text{he}$, ${}^4\text{he}$, n_2 , and xe : line cores and near wings. *Phys. Rev. A*, 56(6), 1997.
- [54] L. D. Schearer, F. D. Colegrove, and G. K. Walters. Large he^3 nuclear polarization. *Phys. Rev. Lett.*, 10:108–110, Feb 1963.

- [55] L. D. Schearer and G. K. Walters. Nuclear spin-lattice relaxation in the presence of magnetic-field gradients. *Phys. Rev.*, 139:A1398–A1402, Aug 1965.
- [56] J. Schmiedeskamp, W. Heil, W. E. Otten, K. R. Kremer, A. Simon, and J. Zimmer. Paramagnetic relaxation of spin polarized ^3He at bare glass surfaces. *The European Physical Journal D - Atomic, Molecular, Optical and Plasma Physics*, 38(3):427–438, 2006.
- [57] J. T. Singh, P. A. M. Dolph, W. A. Tobias, T. D. Averett, A. Kelleher, K. E. Mooney, V. V. Nelyubin, Y. Wang, Y. Zheng, and G. D. Cates. Development of high-performance alkali-hybrid polarized ^3He targets for electron scattering. *Phys. Rev. C*, 91:055205, May 2015.
- [58] C. P. Slichter. *Principles of Magnetic Resonance*.
- [59] W. Smythe. *Static and Dynamic Electricity*.
- [60] A. E. A. M. I. Technologies. <http://www.ableelectropolishing.com>.
- [61] T. V. Tscherbul, P. Zhang, H. R. Sadeghpour, and A. Dalgarno. Anisotropic hyperfine interactions limit the efficiency of spin-exchange optical pumping of ^3He nuclei. *Phys. Rev. Lett.*, 107:023204, Jul 2011.
- [62] M. Wagshul and T. Chupp. Optical pumping of high-density rb with a broadband dye laser and gaalas diode laser arrays: Application to ^3He polarization. *Phys. Rev. A.*, 40, 1989.
- [63] M. Wagshul and T. Chupp. Laser optical pumping of high-density rb in polarized ^3He targets. *Phys. Rev. A*, 49:3854–3869, 1994.

- [64] T. G. Walker and W. Happer. Spin-exchange optical pumping of noble-gas nuclei. *Rev. Mod. Phys.*, 69:629–642, Apr 1997.
- [65] T. G. Walker, I. A. Nelson, and S. Kadlecek. Method for deducing anisotropic spin-exchange rates. *Phys. Rev. A*, 81:032709, Mar 2010.
- [66] T. G. Walker, J. H. Thywissen, and W. Happer. Spin-rotation interaction of alkali-metal–he-atom pairs. *Phys. Rev. A*, 56:2090–2094, Sep 1997.
- [67] D. K. Walter, W. Happer, and T. G. Walker. Estimates of the relative magnitudes of the isotropic and anisotropic magnetic-dipole hyperfine interactions in alkali-metal–noble-gas systems. *Phys. Rev. A*, 58:3642–3653, Nov 1998.
- [68] Y. Zheng. Low field mri and the development of polarized nuclear imaging (pni)-a new imaging modality, 2015.

Appendix A

Appendix title

This is Appendix A.

You can have additional appendices too (*e.g.*, `apdxb.tex`, `apdxc.tex`, *etc.*). If you don't need any appendices, delete the appendix related lines from `thesis.tex` and the file names from `Makefile`.